

Received December 6, 2020, accepted December 27, 2020, date of publication January 27, 2021, date of current version February 16, 2021.

Digital Object Identifier 10.1109/ACCESS.2021.3055034

# Realization of a Simultaneous Position-Stiffness Controllable Antagonistic Joint Driven by Twisted-Coiled Polymer Actuators Using Model Predictive Control

TUAN LUONG<sup>1</sup>, (Graduate Student Member, IEEE), SUNGWON SEO<sup>1</sup>,  
KIHYEON KIM<sup>1</sup>, (Student Member, IEEE), JEONGMIN JEON<sup>1</sup>, FRANCISCO YUMBLA<sup>1,2</sup>,  
JA CHOON KOO<sup>1</sup>, (Member, IEEE), HYOUK RYEOL CHOI<sup>1</sup>, (Fellow, IEEE),  
AND HYUNGPIL MOON<sup>1</sup>, (Member, IEEE)

<sup>1</sup>Department of Mechanical Engineering, Sungkyunkwan University, Suwon 16419, South Korea

<sup>2</sup>Faculty of Mechanical and Production Sciences Engineering, ESPOL Polytechnic University, Guayaquil 9015863, Ecuador

Corresponding author: Hyungpil Moon (hyungpil@skku.edu)


This work was supported by the National Research Foundation of Korea (NRF) Grant funded by the Korean Government (MSIT) under Grant 2020R1A4A1018227.

**ABSTRACT** Stiffness adjustability is one of the key characteristics that help humans achieve safe and reliable motions. This paper aims to realize the simultaneous position-stiffness control of an antagonistic joint driven by a type of super-coiled polymer (SCP) artificial muscles, made from a combination of Spandex and nylon fibers. A nonlinear model that can exhibit the variable stiffness characteristics of the actuator is first proposed. The model, whose parameters are identified and verified experimentally, is suitable for estimating the actuator's stiffness as a function of the length and temperature. Based on a linearized model of the antagonistic joint system, a model predictive control (MPC) is applied to control joint angle and stiffness simultaneously. By controlling both actuators' temperatures, simultaneous position-stiffness control is realized. Our contribution also includes enhancement of MPC control by incorporating time delay estimation to estimate model variations and external disturbances. The control performance is verified with both step command and sinusoidal reference with composite frequencies of 0.02Hz to 0.1Hz. Experimental results show that the system can achieve high accuracy of joint position control performance with the maximum position error of 0.42 degrees while varying joint stiffness 46.5%.

**INDEX TERMS** Model predictive control, spandex, super-coiled polymer actuators, soft actuators, variable stiffness.

## I. INTRODUCTION

Over the past few decades, research efforts have been made to create artificial muscles that possess desirable properties of natural muscles such as lightweight with controllable stiffness, high power to weight ratio, and high dynamic range. As a result, many new soft actuators have been studied, such as pneumatic actuators [1], shape memory alloy actuators [2], shape memory polymer actuators [3], super-coiled polymer (SCP) actuators [4]–[8]. Amongst them, the SCP actuator has drawn attention from many researchers recently.

The associate editor coordinating the review of this manuscript and approving it for publication was Christopher H. T. Lee .

It was found by Haines *et al.* [4] that by continually twisting fishing line threads to an extreme until they form coils, high-performance actuators can be obtained with large stroke, high work density, and high load carrying capabilities. With those interesting properties, low cost, and simple fabrication method, the actuator is a potential substitute for traditional actuation methods, such as electric motors and hydraulic actuators, in various applications, such as rehabilitation and prosthesis fields.

In fact, SCP actuators have been utilized in some bionic designs such as robotic fingers [9], robotic hands [10]–[12], wearable actuators and sensors [13], [14]. Its performance has been improved through extensive research in materials,

fabrication methods, modeling and control. Multiple SCP actuator variations have been created [15]–[18]. Novel fabrication methods and optimal fabrication parameters have been found [18], [19]. The behavior of the actuator can be predicted using both phenomenal models and physics-based models that have been proposed [5], [20]–[23]. Considering its high non-linearity, various position controllers [21], [24]–[26] and force controllers [27] have been developed for this type of actuator. Thanks to those achievements, soft SCP actuators have become a reliable actuation method for many bionic applications such as rehabilitation and prosthesis devices [9]–[11], [13]. However, as most of the works simply use SCP actuators as a source of force, research on utilizing variable stiffness properties of SCP actuators for realization of mechanisms with a compliant behavior, which is the key property for their interaction with their environment, is still an open problem.

It is well-known that active compliance is critical to stabilize our arm motion and to achieve safe working performance when subjected to disturbances [28]. When interacted with external forces, active stiffness control provides joint protection by making the joint less stiff and more compliant, allowing the forces to move the joint passively. Moreover, voluntary movement enabled by active stiffness control helps humans performing dexterous actions and complicated tasks [29], [30]. For examples, when lifting two same kind of objects with different weights, it is required to produce two different levels of joint stiffness with the same joint position. Humans achieve compliant joint actuation by co-contracting antagonistic muscles [29]. The ability to co-contract these antagonistic compliant muscles allows independent control over both joint stiffness and joint position. Similarly, by arranging a pair of SCP actuators in an antagonistic configuration, the same compliant joint as humans' one can be realized. In our previous work [31], a torque-based impedance control for antagonistically driven SCP actuators has been proposed enabling joint angle control with variable impedance. This paper presents an enhanced control method, in which joint stiffness is controlled by adjusting both actuators' temperatures. Through an explicit relationship among the joint stiffness, the joint angle and the actuators' temperatures, it is found that variable joint stiffness values can be obtained at the same joint angle by regulating both actuators' temperatures. Therefore, simultaneous stiffness and position control of the antagonistic joint driven by SCP actuators can be realized.

SCP actuators made from a combination of Spandex and nylon fibers are used in this work. First, the Spandex-nylon SCP actuator is characterized to obtain the relationship between temperature, force, length. Based on the characterization results, a non-linear model of the SCP actuator is developed. The model is capable of capturing the variable stiffness characteristics of the actuator. Its parameters are determined and verified through isometric tests, isothermo tests, dynamics tests and joint stiffness tests.

The simultaneous position-stiffness control is then realized by using linear model predictive control (MPC). The cost function includes joint angle errors and both actuator's temperature errors in order to control joint position and stiffness at the same time. Given the actuator's constraints, MPC is utilized to produce the best control actions at its limits across a discrete finite time horizon. Considering the actuator's highly non-linearity, the time delay estimation (TDE) is designed to compensate for the un-modeled dynamics and external disturbances, which helps increasing the robustness of the controller.

In short, our main contributions include:

- Development of a nonlinear dynamic model that can capture the Spandex-nylon SCP actuator's variable stiffness. Compared with the earlier version of the work [32], this is newly added and plays a critical role in simultaneous stiffness and position control.
- Realization of human like simultaneous position-stiffness control of the antagonistic joint by using MPC. Through integrating temperatures into the MPC's objective function, variable stiffness of the antagonistic joint is obtained by adjusting both actuators' temperatures. In this part, instead of using a fixed forced air environment as in [32], actively controlled cooling is used, meaning cooling fans are switched on/off during controlling.
- Enhancement of linear MPC using TDE. Through estimation error analysis, it is proven that TDE can help compensate the un-modeled dynamics and external disturbances efficiently.

The remaining of this paper is organized as follows. In Section II actuation properties are studied and a nonlinear model for the Spandex-nylon SCP actuator is presented in Section III. Our control design method is discussed in Section IV and experimental results are presented in Section V. We conclude the paper in Section VI.

## II. ACTUATOR PROPERTY CHARACTERIZATION

The actuator utilized in this work is a novel type of SCP actuator made from a combination of Spandex and nylon fibers [18]. In this section, we briefly introduce the actuator, its basic working principle and experimental setups for the actuator's property characterization.

### A. SPANDEX-NYLON TWISTED-COILED ACTUATORS AND ITS WORKING PRINCIPLE

The materials of the actuator are Spandex yarn (Creora®, Hyosung Inc.) and nylon conductive sewing thread (Shieldex™ No. 200121235343B). The fabrication process of the actuator [18] is mostly similar to the one presented in [4] except a pre-stretching process due to the difference between the stiffness of the two fibers. Compared with the SCP actuator made from only conductive nylon fibers, the hybrid type possesses higher tensile stroke (40%) and a smaller temperature range (20°C – 110°C). To increase the actuation force,

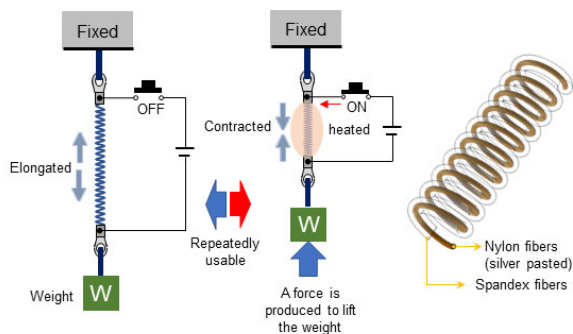


FIGURE 1. Working principle of the actuator.

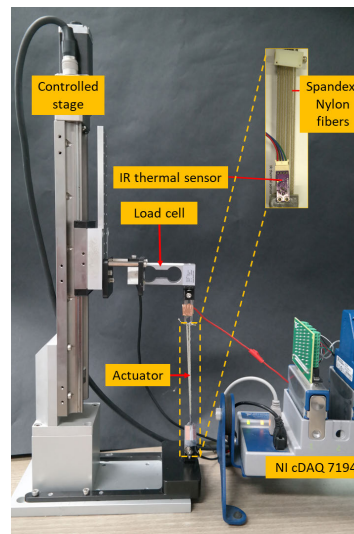
a bundle configuration consisting of 4 single Spandex-nylon SCP fibers is used. In which two fibers were fabricated with the counter-clockwise rotation of the motor, and the other two were fabricated with clockwise rotation. The bundle’s length is equal to the length of each actuator (105 mm at the ambient temperature).

The working principle of the actuator is summarized in Fig. 1. The actuator’s length is changed by heating and cooling, making it a linear actuator. Under the thermal expansion, a contraction in the primary actuator’s coil axis is induced as a change in twist is introduced along the thread. By applying electric current through the silver pasted surface of nylon fibers in the spandex-nylon actuator, Joule heating, a convenient heating method, can be utilized to generate heat to the actuator. When cooling, the actuator elongates again to its original length. The actuator can be cooled by using natural convection or faster forced convection such as forced air. In this work, forced convection using electric fans was used. The contraction and elongation processes can be repeated multiple times.

**B. TEST BED SETUP FOR CHARACTERIZATION OF SPANDEX AND NYLON SCP BUNDLES**

To characterize the SCP actuator, testbeds were developed, as shown in Fig. 2a and Fig 2b. Isothermal and isometric tests are carried out using the experimental setup in Fig. 2a, where the actuator is connected between the testbed and a load cell (CB1A, 2kgf, DACEL CO.). The length of the actuator is accurately controlled by a stepper motor (ZCVL6200-2-N-FN) and a motor controller (DS102, SURUGA SEIKI CO.) with the resolution of 2μm. Actuators are applied power through electrical leads, which are connected to a power supply. The actuator’s temperature was measured with an IR thermal sensor (CJMCU-MLX90614). The temperature and the force values are recorded using NI cDAQ 9174 and Labview.

For the dynamic test, the experimental setup shown in Fig 2b was used, in which the actuator is connected between a load and a load cell (CM, 50kgf, DACEL CO.). The load is attached to a magnetic sensor (MLI-T80, OPKON), which can be used to measure the load’s position. The tem-



(a) Isothermal and isothermal test setup



(b) Dynamic test setup

FIGURE 2. Experimental setup for property characterization of the SCP bundle.

perature was measured with the same IR thermal sensor as discussed prior.

**C. ACTUATOR PROPERTIES**

The same isothermal and isometric testing processes have been conducted to measure the properties of the fabricated SCP actuators. In the isothermal test, strains between 0% and 30% are exerted to the actuator with the controlled stage at different deformation rates of 0.2mm/s, 0.4mm/s, 0.6mm/s, 0.8mm/s. The temperature of the actuator has a variation of ±2°C during the isothermal test; however, it is considered isothermal. Fig. 3 shows the results of the force-strain curves obtained at each temperature with different elongation rates. It is seen from the results that the force-length relationships at the same temperature and different elongation rates are very similar. Therefore,

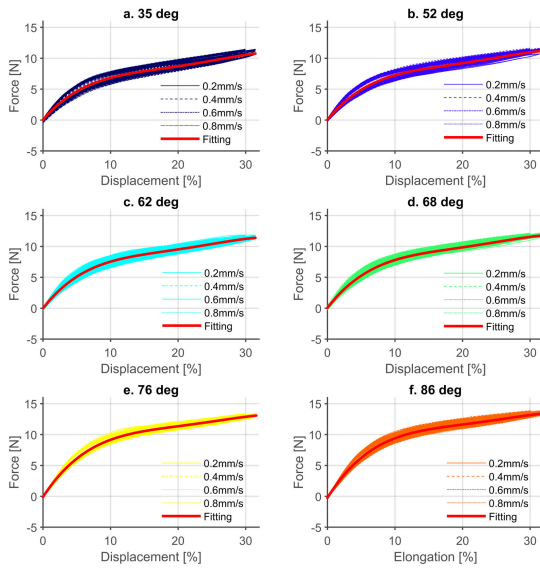


FIGURE 3. A force-strain profile of Spandex-nylon SCP actuators at various temperature conducted at various elongation rate.

it is reasonable to assume that the force-length relationship is independent of the elongation rate. Based on the isothermal test, 4<sup>th</sup> order polynomial fitting was used to find the relationship between strain and force at different temperatures. By taking the derivative of the fitting line, the stiffness of the actuator can be obtained at different temperatures, as shown in Fig. 4. Remarkably, all stiffness curves show an increasing stiffness from 0% to 17% elongation length while almost the same after 17%. Especially, the stiffness at the same elongation point is increased with increasing temperature. At the 0% elongation point, a maximum of 54.6% increase in stiffness can be produced. This phenomenon is also observed in [4], [33]. This stiffened behavior can be explained by contacts between adjacent coils. The large temperature-induced changes in stiffness are very useful to biomimetic applications where variable stiffness is needed.

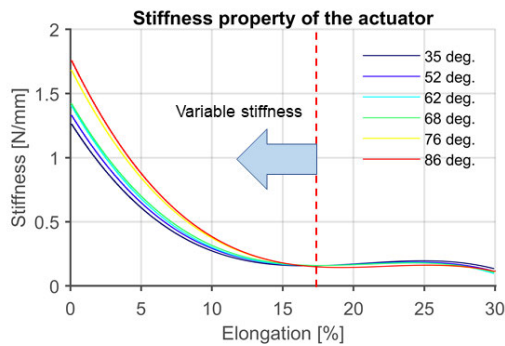


FIGURE 4. Stiffness characterization results.

The isometric test results in Fig. 5 show the linear relationship between the actuator’s temperature and force at fixed elongation points.

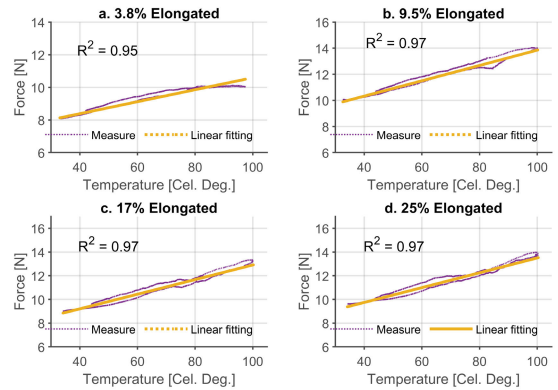


FIGURE 5. Isometric test results.

### III. ACTUATOR MODELING

This section presents the actuator’s model, which includes a thermo-electrical model showing the relationship between the actuation bundle’s temperature and applied power, and a thermo-mechanical model showing the relationship between temperature-force-strain of the bundle.

#### A. THERMO-ELECTRICAL MODEL

Similar to a single SCP actuator, the thermo-electrical model of a SCP bundle can be described by the following Joule heating model:

$$C_{th} \frac{dT(t)}{dt} = P(t) - \lambda(T - T_{amb}) \quad (1)$$

where  $C_{th}$  is the thermal mass of the actuator,  $P(t) = \frac{V^2}{R}$  is the Joule heating that is applied to the bundle, and  $\lambda$  is the heat transfer coefficient of the bundle in its ambient environment. The same method here is also used to find  $C_{th}$  and  $\lambda$  through experimental data. To increase the cooling speed, electric fans are used. The parameters obtained from the experimental data are shown in Table 1.

TABLE 1. Spandex-nylon SCP system parameters.

Parameter	Value
Actuator’s mass $m$	14 (g)
Resistance $R$	7.5 ( $\Omega$ )
Thermal mass (fan cooling) $C_{th1}, C_{th2}$	5.85 ( $J/^\circ C$ )
Heat transfer coefficient (fan cooling) $\lambda_1, \lambda_2$	0.71 ( $W/^\circ C$ )
pulley radius $r$	0.015 (mm)
$k_1^{(1)}, k_1^{(2)}$	0.0233 ( $^\circ C$ )
$k_2^{(1)}, k_2^{(2)}$	-80.528 ( $N/(m^\circ C)$ )
$k_3^{(1)}, k_3^{(2)}$	0.2452 ( $N/m$ )
$k_4^{(1)}, k_4^{(2)}$	0.1424 ( $N/mm$ )
$k_5^{(1)}, k_5^{(2)}$	0.0043 ( $N/^\circ C$ )
$k_6^{(1)}, k_6^{(2)}$	0.1843 (N)

**B. STIFFNESS MODEL**

Based on the stiffness characterization shown in Fig. 4, a stiffness model is proposed as follows

$$K = k_1 \frac{T - k_2}{1 + e^{k_3x}} + k_4 \quad (2)$$

where  $T$  is the actuator’s temperature and  $k_i$  are constants. The explicit model shows stiffness’s dependence on the actuator’s elongation and temperature. The model’s parameters are identified based on the experimental results. Fig. 6 shows a good fit of the model to the variable stiffness behavior of the actuator with high correlation coefficients.

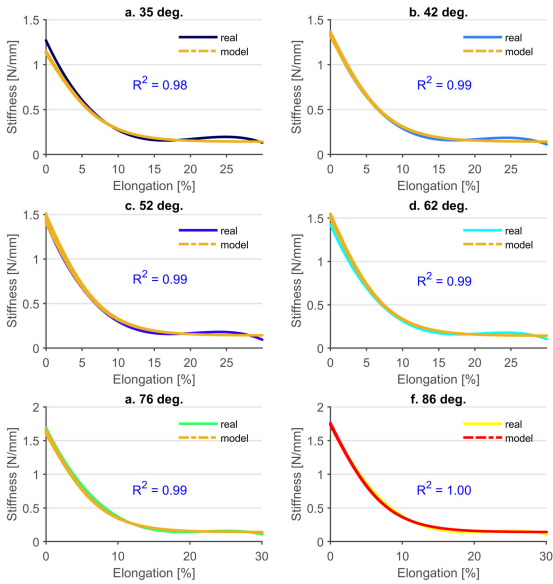


**FIGURE 6. Stiffness model parameter identification results.**

**C. THERMO-MECHANICAL MODEL**

From the isometric test results, it is seen that the elongation independent temperature effect on the actuator’s force can be expressed by the following equation

$$F_{temp} = \alpha(T - T_{amb}) + \beta \quad (3)$$

where  $\alpha$  and  $\beta$  are constants.

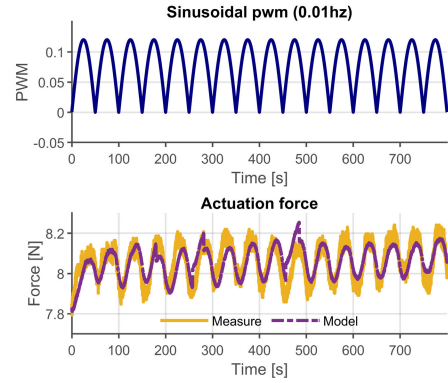
The thermo-mechanical model then can be obtained by integrating the stiffness model with respect to elongation and combining with the elongation independent temperature effect term in Eq. (3), yielding the following equation

$$F = k_1(T - k_2)(x - \ln(1 + e^{k_3x}) + \ln 2) + k_4x + k_5(T - T_{amb}) + k_6 \quad (4)$$

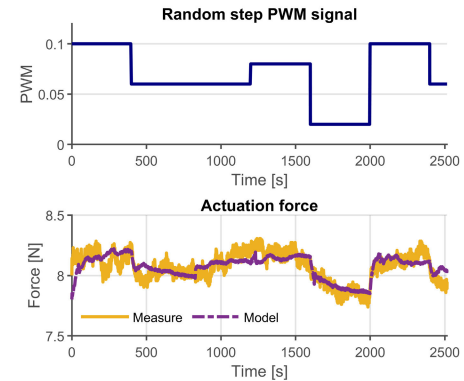
where  $T$  is the actuator’s temperature and  $x$  is its elongated length.  $k_i$  for  $i = 1-6$  are constants and  $k_i$  for  $i = 1-4$  can be obtained directly from the integration of the stiffness model with respect to elongation.  $k_5$  and  $k_6$  are identified based on the isometric test shown in Fig. 5. The parameters for the thermo-mechanical model are listed in Table 1.

**D. MODEL VERIFICATION**

To verify the model, different voltages with both sinusoidal and step forms are applied to the actuator in the experimental setup in Fig. 2b. A load of 0.8kg was used. Modeling results can be seen in Fig. 7 verifying the effectiveness of the proposed model to predict the actuator’s dynamic behavior.



**(a) Sinusoidal waveform PWM input with frequency of 0.03Hz**



**(b) Random step PWM input**

**FIGURE 7. Modeling verification of the Spandex-nylon actuator.**

Moreover, the stiffness model was also verified by testing the stiffness of the antagonistic joint at the joint angle of 10 degrees when varying each actuator’s temperatures. During the test, each actuator’s temperature is controlled and gradually increased within its limits so that the joint angle is regulated at 10 degrees. At each set of the two actuators’ temperatures, the joint stiffness is evaluated by manually rotating the joint about its axis a constant angle.

The change in joint torque is obtained by two load cells connected with the two actuators. The joint stiffness model can be derived based on each actuator’s stiffness model as follows

$$K_{joint} = r^2(K_1 + K_2) \quad (5)$$

where  $K_i, i = 1, 2$  are stiffness of actuator 1 and 2, respectively. They are estimated based on the stiffness model in Eq. 2. The results shown in Fig. 8 again confirm the capability

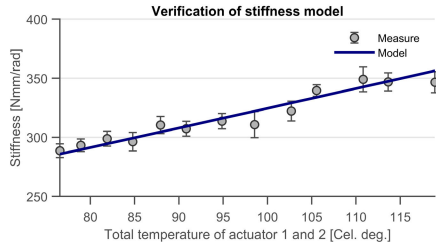


FIGURE 8. Joint stiffness verification at 10 degree.

of the model to capture the variable stiffness behavior of the actuator.

E. ANTAGONISTIC JOINT MODEL

The equation of motion of antagonistic joint is given as follows.

$$J\ddot{\theta} = (F_2 - F_1)r \tag{6}$$

where  $J$  is the inertia moment of the antagonistic joint,  $\theta$  is the joint angle,  $F_i$  is the force applied by actuator  $i$  ( $i = 1, 2$ ) and  $r$  is the pulley radius.

From the thermo-electrical model (1), thermo-mechanical model (4) of the bundle and the antagonistic joint model (6), one can have the state equation of the system in the form of Eq. 8

$$\dot{x} = f(x, u) \tag{7}$$

where  $x = [\theta, \dot{\theta}, T_1 - T_{amb}, T_2 - T_{amb}]^T$ ,  $u = [u_1, u_2]^T$ ,  $T_i$  is the temperature of the actuator  $i$  ( $i = 1, 2$ ),  $T_{amb} = 25^\circ C$  is the ambient temperature.

From Eq. 7, a linearized model can be obtained by linearizing Eq. 7 around ( $u = 0, x = 0$ )

$$\dot{x} = A_c x + B_c u + d_c \tag{8}$$

where  $d_c$  is the disturbance vector,  $A_c, B_c$  are Jacobian matrices and can be obtained as follows

$$A_c = \left. \frac{\partial f}{\partial x} \right|_{(u=0, x=0)} \tag{9}$$

$$B_c = \left. \frac{\partial f}{\partial u} \right|_{(u=0, x=0)} \tag{10}$$

The detailed derivation of the entries of matrices  $A_c, B_c$  can be found in Appendix A.

IV. MODEL PREDICTIVE CONTROL

MPC is an advanced control technique that uses online optimization performed over a prediction horizon to calculate the best control actions. One of the advantages of MPC is the integration of the system model and constraints into a single controller. Although the optimization is run over the prediction horizon, only the first control action is taken. The optimization is then re-calculated after receiving feedback from the current system in the next time step.

The continuous-time system described in Eq. 8 can be converted to an equivalent discrete-time system using a standard zero-order hold discretization procedure yielding

$$x_{k+1} = A_d x_k + B_d u_k + d_k \tag{11}$$

where

$$\begin{aligned} A_d &= e^{A_c T_s} \\ B_d &= \int_0^{T_s} e^{A_c \tau} B_c d\tau \\ d_k &= \int_0^{T_s} e^{A_c \tau} d_c(kT_s + T_s - \tau) d\tau \end{aligned} \tag{12}$$

Here,  $T_s$  is the sampling time.

The MPC problem can be formulated as

$$\begin{aligned} \min_{u_i} \quad & \sum_{i=k}^{k+N_p-1} \xi(\theta_i^d - \theta_i)^2 \\ & + \mu u_i^T u_i + \gamma_1 (T_{1i} - T_{1i}^d)^2 + \gamma_2 (T_{2i} - T_{2i}^d)^2 \end{aligned} \tag{13}$$

subjected to:

$$x_{i+1} = A_i x_i + B_i u_i + \hat{d}_i \tag{14}$$

$$\begin{aligned} u_{i,min} &\leq u_i \leq u_{i,max} \\ i &= k, \dots, k + N_p - 1 \end{aligned} \tag{15}$$

where  $\theta$  is the joint angle,  $T_i, i = 1, 2$  are temperature of actuator 1 and 2, respectively. Superscript  $(.)^d$  is used to indicate the reference value of a variable.  $u_{i,min}$  and  $u_{i,max}$  are minimum and maximum values of input vector  $u_i, i = k, \dots, k + N_p - 1$ .

It is noted here that the joint stiffness is controlled through adjusting both actuators' temperatures. The target temperatures of two actuators are calculated as follows:

$$\begin{aligned} \text{if } (\theta_i^d \geq 0) : \\ T_{1i}^d &= T_0 + T_{amb}, T_{2i}^d = K\theta_i^d + T_0 + T_{amb} \end{aligned}$$

else:

$$T_{1i}^d = K|\theta_i^d| + T_0 + T_{amb}, T_{2i}^d = T_0 + T_{amb} \tag{16}$$

where  $T_0$  is an offset target temperature. The target temperature relates the desired joint angle through a constant  $K$ .  $N_p$  is the prediction horizon,  $\xi, \mu, \gamma_1, \gamma_2$  are scalar weights which penalize input deviations, state deviation, and actuator temperature 1 and 2, respectively.  $u_{min} \in \mathbb{R}^2, u_{max} \in \mathbb{R}^2$ . The optimization problem returns  $u = [u_k, u_{k+1}, \dots, u_{k+N_p-1}]^T$ .

The disturbance vector  $d_{k+j}, j = 0 \dots N_p - 1$  is estimated by

$$\hat{d}_{k+j} = d_{k-1}, j = 0 \dots N_p - 1 \tag{17}$$

where  $d_{k-1} = x_k - A_d x_{k-1} - B_d u_{k-1}$ . It can be shown in Appendix B that the error between the actual and estimated values of  $d_{k+j}$  is  $\alpha + \mathcal{O}(T_s)$ , where  $\alpha$  is a positive number. Therefore, by reducing the sampling time, better disturbance estimation performance can be achieved. As the performance

of MPC relies on the system's model, a more accurate model and estimation will provide better prediction to MPC, therefore increasing the system's performance.

It is observed that below the power limit level, some high power levels still break the actuator due to overheating at a steady state. Therefore, instead of using constant power limits for the MPC, we calculate the instant power limits of the actuator based on the actuator's maximum working temperature, its current temperature, and heat transfer model.

From the discrete model of heat transfer equation in section III-A, the power constraint can be set as follows

$$P_{k,max} = C_{th} \frac{T_{max} - T_k}{T_s} + \lambda(T_k - T_{amb}) \quad (18)$$

In this work, cooling fans are used to increase the cooling speed of the actuator. However, the forced air environment (meaning fans are on) is not fixed as in [32]. Instead, the cooling fans are actively on/off controlled independently for each actuator. The fans are switched on only when their associated actuators' temperatures are higher than their temperature limits or desired values, and the fan state-changing permission flag is on. The permission flag is enabled in every predetermined time interval. The time interval should be chosen sufficiently long to guarantee the linear MPC controlled system's stability when switched between different linear systems [34]. Here, changes in the SCP actuator system due to switching cooling fans are the changes in heat transfer parameter values ( $\lambda^{(i)}$ ,  $C_{th}^{(i)}$ ) involved in the state equation.

CVXGEN [35] is a web-based tool for generating convex optimization solvers that can run up to 300Hz. It is widely used in both linear invariant and dynamic MPC control [36] of small scale problems. We utilized CVXGEN to generate a solver for our optimization problem. The code is then converted to .dll file to be used in Labview for experiments.

## V. CONTROL IMPLEMENTATION

To verify the control design, a series of experiments have been carried out on the experimental setup in Fig. 9. In this setup, two bundles of Spandex-nylon actuators are arranged in an antagonistic configuration. Each actuation bundle with an integrated thermal sensor is connected with the base at one end through a load cell (CM, 50kgf, DACEL CO.) and connected with a round pulley through an in-extensible wire at the other end. A general power supply (30V, 5A) was used to supply power to actuators. The current is kept within 3A as a safety limit. The power applied to the actuator is distributed from the power supply through a motor drive module (DC Motor Driver 2 × 15A-Lite) controlled by PWM signals sent from a NI cDAQ 9174 module. The joint encoder is measured using (ATM203-1024). The sampling frequency is 15Hz. The controller parameters were chosen as:  $\xi = 10^{-3}$ ,  $\mu = 4000$ ,  $\gamma = 10$ ,  $K = 100$ . The prediction horizon of the MPC control is chosen as  $N_p = 5$ . The fan changing permission time is set as  $N_p$  times of the sampling time. In the

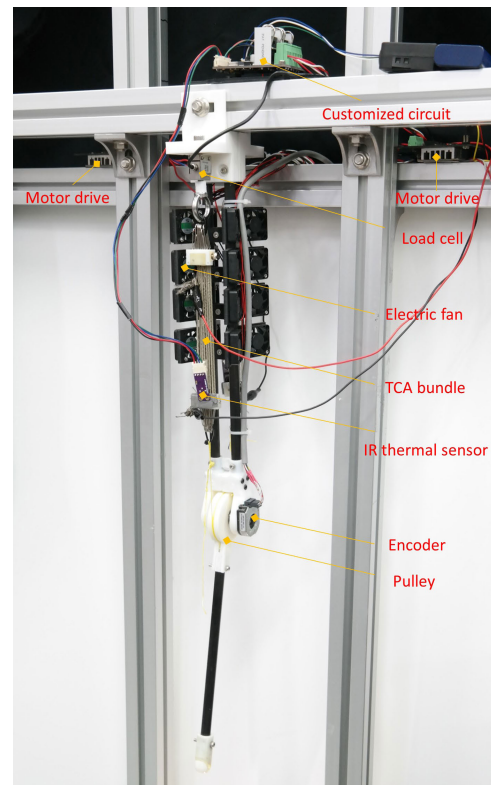


FIGURE 9. One DoF antagonistic joint driven by SCP bundle actuators.

experiment, a weight of 10g was added to the end of the arm as an external disturbance source. The maximum temperature of each actuator is limited within 85°C.

## A. EXPERIMENTAL RESULTS

In the first experiment, the ability of the controller to hold the joint at a constant angle while changing the joint stiffness was examined. A joint angle reference of 5 degrees was assigned and both actuators' temperature reference values are varied in steps through the assignment of the target temperature offset  $T_0$  varying from 2°C to 13°C. From Eq. 2, when the joint angle is fixed, joint stiffness is proportional to the target temperature offset. Experimental performances are shown from Fig. 10. While the desired varying temperatures of two actuators are followed (corresponding to a varying joint stiffness of 30.1% (233.7Nmm/rad to 304.47Nmm/rad)), the angle error remains less than 0.3 degrees at steady state. The result indicates that the proposed controller can reliably adjust the joint stiffness while maintaining a relatively constant joint angle.

Whereas Fig. 11 and Fig. 12 depict results from a simultaneous position and variable stiffness tracking experiment. In Fig. 11, the joint angle reference is stepped from 0 to 20 degrees while the target temperature offset reference  $T_0$  is stepped between 0°C and 13°C. It can be seen that similar to the first experiment, both desired step temperatures and step joint angle can be followed. The joint angle error at the

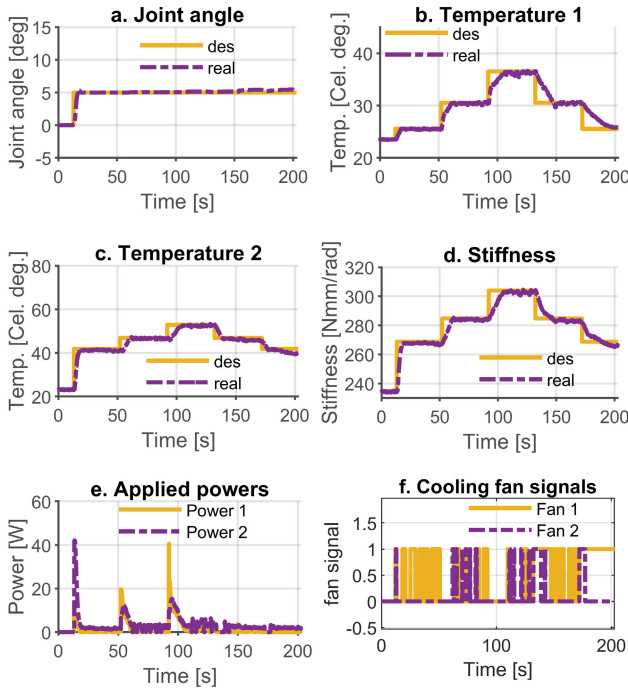


FIGURE 10. Experimental results for keeping a constant joint angle while varying a multi-step temperature, which is related to stiffness.

steady-state remains less than 0.57 degrees while the corresponding joint stiffness was varied 33.5% (233.7Nmm/rad to 312.2Nmm/rad).

Fig. 12 shows the results when both joint angle and target temperature offset reference are both sinusoidal waveforms. The joint angle reference is assigned via a sinusoidal waveform with composite frequencies of 0.02Hz and 0.1Hz, and the temperature offset is commanded to follow a sinusoidal reference with a frequency of 0.01Hz, which results in a sinusoidal waveform with composite frequencies of 0.01Hz, 0.02Hz, and 0.1Hz for the required temperatures. Although the actuators' temperatures are varied largely (corresponding to a joint stiffness variation of 46.5% (233.7Nmm/rad to 342.5Nmm/rad)), the steady-state tracking error is maintained less than 0.46 degrees, which shows the controller's effectiveness. The results, shown in Fig. 11 and Fig. 12, therefore, verify the controller's ability to achieve simultaneous position-stiffness tracking control.

More details of the experimental results plotted in Fig. 10-Fig. 12 are shown in Table 2. The results obtained in this work are compared with those in our previous work [32]. It is obvious that the current work achieves better control performance in terms of mean joint error, maximum joint error, rising time, and overshoot. The mean joint error and maximum joint error are reduced by 45.7% and 42.9%, respectively. The overshoot and rising time are improved 120% and 42.5%, respectively.

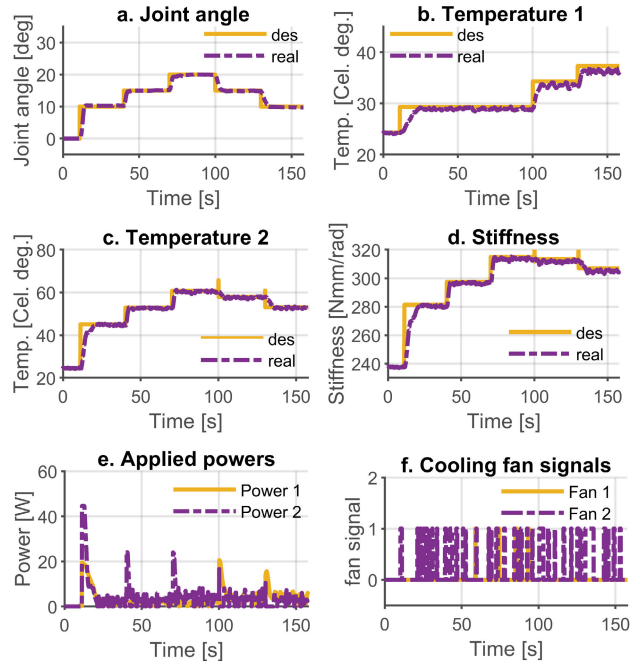


FIGURE 11. Experimental results for controlling a multi-step joint angle and multi-step temperatures simultaneously.

TABLE 2. Control performance comparisons.

	Previous work [32]	Current work
Mean joint error (deg)	0.51±0.06	0.35±0.15
Max error (deg)	0.60	0.42
Rising time (s)	4.83±1.2	3.39±0.89
Overshoot (s)	0.53±0.4	0.24±0.07

B. DISCUSSIONS

Experimental results verified the capability of our proposed control frame to control simultaneously position-stiffness of the antagonistic system driven by Spandex-nylon bundles. At its heart, the model predictive control plays an important role in providing model-based predictive behaviors, which gives the best control actions over the prediction horizon and takes into account the physical constraints of the actuators. The time delay estimation also contributes to the controller's performance by helping compensate for the actuator's nonlinear properties and external disturbances.

It was shown in [37] that forced air cooling helps reduce time constant and improve linearity of the actuator's dynamics. However, constant forced air cooling brings another cost. With the same applied power, the reduced time constant is also associated with a lower steady-state temperature due to increased loss of energy. Therefore, for the same joint position target, higher power is needed to provide enough heat to



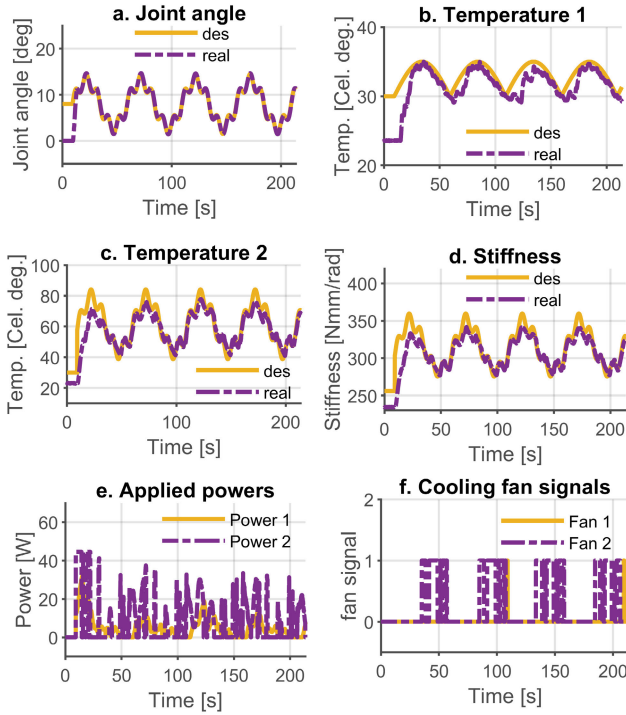


**FIGURE 12.** Experimental results of controlling a sinusoidal angle (with composite frequencies of 0.02hz and 0.1hz) and sinusoidal temperatures (0.01hz) simultaneously.

the actuator than when using a natural cooling environment. This is not only energy efficient but also increases the risk of breaking the actuator. When the actuator is heated, turning off the forced air will make it faster to obtain the desired temperature, thus achieving a faster response towards the desired position and stiffness. Indeed, it is verified that active cooling helped decrease the rising time compared with our previous work [32], where a constant forced air environment is used.

Since the cooling speed significantly affects the response of SCP actuators, the system’s performance can also be improved by using other enhanced cooling methods actively. Some faster cooling candidates compared with fan cooling are water, pressurized airs, and Peltier devices. However, as these methods require bulky structures, more compact design of SCP actuators driven mechanisms with embedded active cooling structures are also needed. Those compact, stiffness and position controllable modules will further help improve the practical applicability of the SCP actuator. For example, a modular approach similar to [38] can be used to faster create a more complex robot structure from multiple units of the SCP module.

## VI. CONCLUSION

In this paper, a novel nonlinear thermo-mechanical model for a type of SCP actuators made from Spandex and nylon fibers was presented. Experiments confirm the capability of

the model to capture the actuator’s variable stiffness and dynamics behavior. This enabled us to obtain the antagonistic joint position reference and simultaneously adjust the joint’s stiffness through MPC control. The active stiffness controllability, which is a crucial characteristic of human muscles, thus makes Spandex-nylon actuators a suitable artificial muscle to be used efficiently in bio-mimetic applications that interact with humans.

Based on this work, the next steps will be the extension to multi-DOF Spandex-nylon bundle driven bionic hands and bionic arms with controllable stiffness.

## A. JACOBIAN MATRICES

$$A_c[1, 2] = \left. \frac{\partial f_1}{\partial x_2} \right|_{(u=0, x=0)} = 1 \quad (19)$$

$$A_c[2, 1] = \left. \frac{\partial f_2}{\partial x_1} \right|_{(u=0, x=0)} = \frac{r^2}{J} \left[ -k_1^{(2)}(x_4 - k_2^{(2)})(1 - k_3^{(2)}) \frac{e^{k_3^{(2)}(l_{20} - rx_1)}}{1 + e^{k_3^{(2)}(l_{20} - rx_1)}} - k_1^{(2)}(x_4 - k_2^{(2)})(1 - k_3^{(1)}) \frac{e^{k_3^{(1)}(l_{10} + rx_1)}}{1 + e^{k_3^{(1)}(l_{10} + rx_1)}} - k_4^{(2)} - k_4^{(1)} \right]_{(u=0, x=0)} = \frac{r^2}{J} \left[ (k_1^{(2)}k_2^{(2)} + k_1^{(1)}k_2^{(1)}) - (k_1^{(2)}k_2^{(2)}k_3^{(2)} \frac{e^{k_3^{(2)}l_{20}}}{1 + e^{k_3^{(2)}l_{20}}} + k_1^{(1)}k_2^{(1)}k_3^{(1)} \frac{e^{k_3^{(1)}l_{10}}}{1 + e^{k_3^{(1)}l_{10}}}) - (k_4^{(2)} + k_4^{(1)}) \right] \quad (20)$$

$$A_c[2, 3] = \left. \frac{\partial f_2}{\partial x_3} \right|_{(u=0, x=0)} = -\frac{r^2}{J} \left[ k_1^{(1)} \left( (l_{10} + rx_1) - \ln(1 + e^{k_3^{(1)}(l_{10} + rx_1)}) + \ln 2 \right) + k_5^{(1)} \right]_{(u=0, x=0)} = -\frac{r^2}{J} \left[ k_1^{(1)} \left( l_{10} - \ln(1 + e^{k_3^{(1)}l_{10}}) + \ln 2 \right) + k_5^{(1)} \right] \quad (21)$$

$$A_c[2, 4] = \left. \frac{\partial f_2}{\partial x_4} \right|_{(u=0, x=0)} = \frac{r^2}{J} \left[ k_1^{(2)} \left( (l_{20} - rx_1) - \ln(1 + e^{k_3^{(2)}(l_{20} - rx_1)}) + \ln 2 \right) + k_5^{(2)} \right]_{(u=0, x=0)} = \frac{r^2}{J} \left[ k_1^{(2)} \left( l_{20} - \ln(1 + e^{k_3^{(2)}l_{20}}) + \ln 2 \right) + k_5^{(2)} \right] \quad (22)$$

$$\begin{aligned}
 A_c[3, 3] &= \frac{\partial f_3}{\partial x_3} \Big|_{(\mathbf{u}=\mathbf{0}, \mathbf{x}=\mathbf{0})} \\
 &= -\frac{\lambda^{(1)}}{Cth^{(1)}} \tag{23}
 \end{aligned}$$

$$\begin{aligned}
 A_c[4, 4] &= \frac{\partial f_4}{\partial x_4} \Big|_{(\mathbf{u}=\mathbf{0}, \mathbf{x}=\mathbf{0})} = -\frac{\lambda^{(2)}}{Cth^{(2)}} \tag{24}
 \end{aligned}$$

$$\begin{aligned}
 B_c[3, 1] &= \frac{\partial f_3}{\partial u_1} \Big|_{(\mathbf{u}=\mathbf{0}, \mathbf{x}=\mathbf{0})} = \frac{1}{Cth^{(1)}} \tag{25}
 \end{aligned}$$

$$\begin{aligned}
 B_c[4, 2] &= \frac{\partial f_3}{\partial u_2} \Big|_{(\mathbf{u}=\mathbf{0}, \mathbf{x}=\mathbf{0})} = \frac{1}{Cth^{(2)}} \tag{26}
 \end{aligned}$$

All other elements are zero. Here, superscripts  $(\cdot)^{(i)}$ ,  $i = 1, 2$  are used to indicate actuator 1 and 2, respectively.  $l_{i0}$ ,  $l_i$  are the initial elongation and current elongation of the actuator  $i$  ( $i = 1, 2$ ), respectively.

Each actuator's elongation and joint angle is related as follows

$$l_1 = l_{10} + r\theta \tag{27}$$

$$l_2 = l_{20} - r\theta \tag{28}$$

### B. TIME DELAY ESTIMATION ERROR

The disturbance term  $\mathbf{d}$  can be separated into model uncertainties and external disturbances, which can be represented as

$$\mathbf{d} = \mathbf{h}(\mathbf{x}) + \mathbf{d}_{ext} \tag{29}$$

where  $\mathbf{h}(\mathbf{x})$  is the sum of model uncertainties and  $\mathbf{d}_{ext}$  is external disturbance.

Since it is well-known that many hysteresis operators are Lipschitz continuous [39], considering the hysteresis properties of the SCP actuator as shown in [21], it can be assumed that  $\mathbf{h}(\mathbf{x})$  is Lipschitz continuous. From the Lipschitz continuous condition, one obtains

$$\begin{aligned}
 \mathbf{e}_{h,k} &= \mathbf{h}_k - \mathbf{h}_{k-1} \\
 &= \int_0^{T_s} \mathbf{A}_e e^{\tau} (\mathbf{h}(kT_s + T_s - \tau) - \mathbf{h}(kT_s - \tau)) d\tau \\
 &= \mathcal{O}(T_s) \tag{30}
 \end{aligned}$$

Then

$$\begin{aligned}
 \mathbf{e}_{h,k+j} &= \mathbf{h}_{k+j} - \mathbf{h}_{k-1} \\
 &= (\mathbf{h}_{k+j} - \mathbf{h}_{k+j-1}) + (\mathbf{h}_{k+j-1} - \mathbf{h}_{k+j-2}) \\
 &\quad + \dots + (\mathbf{h}_k - \mathbf{h}_{k-1}) = \mathcal{O}(T_s), j = 0 \dots N_p - 1 \tag{31}
 \end{aligned}$$

The external disturbance term  $\mathbf{d}_{ext}$  can also be separated into continuous and discontinuous terms.

$$\mathbf{d}_{ext} = \mathbf{d}_{cont} + \mathbf{d}_{disc} \tag{32}$$

It is assumed here that  $\mathbf{e}_{disc,j} = \mathbf{d}_{disc,k+j} - \mathbf{d}_{disc,k-1}$  is bounded by  $|\mathbf{e}_{disc,i}| \leq \alpha$ , where  $\alpha$  is a positive value.

If  $\mathbf{d}_{cont}(t)$  and its time derivative is bounded,  $\mathbf{e}_{cont,k} = \mathbf{d}_{cont,k} - \mathbf{d}_{cont,k-1} = \mathcal{O}(T_s^2)$  [40]. Therefore,  $\mathbf{e}_{cont,k+j} = \mathbf{d}_{cont,k+j} - \mathbf{d}_{cont,k-1} = \mathcal{O}(T_s^2)$ .

In summary, the time delay estimation error  $\mathbf{e}_{k,j} = \mathbf{d}_{k+j} - \mathbf{d}_{k-1}$  is  $\alpha + \mathcal{O}(T_s)$

### REFERENCES

- [1] R. M. Robinson, C. S. Kothera, R. M. Sanner, and N. M. Wereley, "Nonlinear control of robotic manipulators driven by pneumatic artificial muscles," *IEEE/ASME Trans. Mechatronics*, vol. 21, no. 1, pp. 55–68, Feb. 2016.
- [2] D. Grant and V. Hayward, "Variable structure control of shape memory alloy actuators," *IEEE Control Syst. Mag.*, vol. 17, no. 3, pp. 80–88, Jun. 1997.
- [3] A. Lendlein and O. E. C. Gould, "Reprogrammable recovery and actuation behaviour of shape-memory polymers," *Nature Rev. Mater.*, vol. 4, no. 2, pp. 116–133, Feb. 2019.
- [4] C. S. Haines et al., "Artificial muscles from fishing line and sewing thread," *Science*, vol. 343, no. 6173, pp. 868–872, Feb. 2014.
- [5] M. C. Yip and G. Niemeyer, "High-performance robotic muscles from conductive nylon sewing thread," in *Proc. IEEE Int. Conf. Robot. Autom. (ICRA)*, May 2015, pp. 2313–2318.
- [6] S. M. Mirvakili, A. R. Ravandi, I. W. Hunter, C. S. Haines, N. Li, J. Foroughi, S. Naficy, G. M. Spinks, R. H. Baughman, and J. D. W. Madden, "Simple and strong: Twisted silver painted nylon artificial muscle actuated by joule heating," *Proc. SPIE*, vol. 9056, Mar. 2014, Art. no. 90560I.
- [7] S. Kianzad, M. Pandit, A. Bahi, A. Rafiee, F. Ko, G. M. Spinks, and J. D. W. Madden, "Nylon coil actuator operating temperature range and stiffness," *Proc. SPIE*, vol. 9430, Apr. 2015, Art. no. 94301X.
- [8] T. A. Luong, S. Seo, J. C. Koo, H. R. Choi, and H. Moon, "Differential hysteresis modeling with adaptive parameter estimation of a super-coiled polymer actuator," in *Proc. 14th Int. Conf. Ubiquitous Robots Ambient Intell. (URAI)*, Jun. 2017, pp. 607–612.
- [9] L. Wu, M. J. de Andrade, R. S. Rome, C. Haines, M. D. Lima, R. H. Baughman, and Y. Tadesse, "Nylon-muscle-actuated robotic finger," *Proc. SPIE*, vol. 9431, Apr. 2015, Art. no. 94310I.
- [10] L. Saharan, M. J. de Andrade, W. Saleem, R. H. Baughman, and Y. Tadesse, "IGrab: Hand orthosis powered by twisted and coiled polymer muscles," *Smart Mater. Struct.*, vol. 26, no. 10, Oct. 2017, Art. no. 105048.
- [11] L. Wu, M. J. de Andrade, L. K. Saharan, R. S. Rome, R. H. Baughman, and Y. Tadesse, "Compact and low-cost humanoid hand powered by nylon artificial muscles," *Bioinspiration Biomimetics*, vol. 12, no. 2, Feb. 2017, Art. no. 026004.
- [12] L. Saharan and Y. Tadesse, "Robotic hand with locking mechanism using TCP muscles for applications in prosthetic hand and humanoids," *Proc. SPIE*, vol. 9797, Apr. 2016, Art. no. 97970V.
- [13] C. Choi, J. M. Lee, S. H. Kim, S. J. Kim, J. Di, and R. H. Baughman, "Twistable and stretchable sandwich structured fiber for wearable sensors and supercapacitors," *Nano Lett.*, vol. 16, no. 12, pp. 7677–7684, Dec. 2016.
- [14] M. Hiraoka, K. Nakamura, H. Arase, K. Asai, Y. Kaneko, S. W. John, K. Tagashira, and A. Omote, "Power-efficient low-temperature woven coiled fibre actuator for wearable applications," *Sci. Rep.*, vol. 6, no. 1, Dec. 2016, Art. no. 36358.
- [15] C. Xiang, H. Yang, Z. Sun, B. Xue, L. Hao, M. D. A. Rahoman, and S. Davis, "The design, hysteresis modeling and control of a novel SMA-fishing-line actuator," *Smart Mater. Struct.*, vol. 26, no. 3, Mar. 2017, Art. no. 037004.
- [16] S. Aziz, S. Naficy, J. Foroughi, H. R. Brown, and G. M. Spinks, "Twist-coil coupling fibres for high stroke tensile artificial muscles," *Sens. Actuators A, Phys.*, vol. 283, pp. 98–106, Nov. 2018.
- [17] S. Y. Yang, K. H. Cho, Y. Kim, M.-G. Song, H. S. Jung, J. W. Yoo, H. Moon, J. C. Koo, J.-D. Nam, and H. R. Choi, "High performance twisted and coiled soft actuator with spandex fiber for artificial muscles," *Smart Mater. Struct.*, vol. 26, no. 10, Oct. 2017, Art. no. 105025.
- [18] K. Kim, K. H. Cho, H. S. Jung, S. Y. Yang, Y. Kim, J. H. Park, H. Jang, J. Nam, J. C. Koo, H. Moon, J. W. Suk, H. Rodriguez, and H. R. Choi, "Double helix twisted and coiled soft actuator from spandex and nylon," *Adv. Eng. Mater.*, vol. 20, no. 11, Nov. 2018, Art. no. 1800536.

- [19] T. Li, Y. Wang, K. Liu, H. Liu, J. Zhang, X. Sheng, and D. Guo, "Thermal actuation performance modification of coiled artificial muscle by controlling annealing stress," *J. Polym. Sci. B, Polym. Phys.*, vol. 56, no. 5, pp. 383–390, Mar. 2018.
- [20] A. Abbas and J. Zhao, "A physics based model for twisted and coiled actuator," in *Proc. IEEE Int. Conf. Robot. Autom. (ICRA)*, May 2017, pp. 6121–6126.
- [21] T. A. Luong, K. H. Cho, M. G. Song, J. C. Koo, H. R. Choi, and H. Moon, "Nonlinear tracking control of a conductive supercoiled polymer actuator," *Soft Robot.*, vol. 5, no. 2, pp. 190–203, Apr. 2018.
- [22] T. Arakawa, K. Takagi, K. Tahara, and K. Asaka, "Position control of fishing line artificial muscles (coiled polymer actuators) from nylon thread," *Proc. SPIE*, vol. 9798, Apr. 2016, Art. no. 97982W.
- [23] L. Sutton, H. Moein, A. Rafiee, J. D. W. Madden, and C. Menon, "Design of an assistive wrist orthosis using conductive nylon actuators," in *Proc. 6th IEEE Int. Conf. Biomed. Robot. Biomechtron. (BioRob)*, Jun. 2016, pp. 1074–1079.
- [24] M. Suzuki and N. Kamamichi, "Control of twisted and coiled polymer actuator with anti-windup compensator," *Smart Mater. Struct.*, vol. 27, no. 7, Jul. 2018, Art. no. 075014.
- [25] T. Luong, K. Kim, S. Seo, J. H. Park, Y. Kim, S. Y. Yang, K. H. Cho, J. C. Koo, H. R. Choi, and H. Moon, "Modeling and position control of a high performance twisted-coiled polymer actuator," in *Proc. 15th Int. Conf. Ubiquitous Robots (UR)*, Jun. 2018, pp. 73–79.
- [26] J. van der Weijde, H. Vallery, and R. Babuska, "Closed-loop control through self-sensing of a joule-heated twisted and coiled polymer muscle," *Soft Robot.*, vol. 6, no. 5, pp. 621–630, 2019.
- [27] C. Wu and W. Zheng, "Position and force control of a twisted and coiled polymeric actuator," *IEEE Access*, vol. 8, pp. 137226–137234, 2020.
- [28] E. Burdet, R. Osu, D. W. Franklin, T. E. Milner, and M. Kawato, "The central nervous system stabilizes unstable dynamics by learning optimal impedance," *Nature*, vol. 414, no. 6862, pp. 446–449, 2001.
- [29] N. Hogan, "Adaptive control of mechanical impedance by coactivation of antagonist muscles," *IEEE Trans. Autom. Control*, vol. AC-29, no. 8, pp. 681–690, Aug. 1984.
- [30] J. A. Kelso and K. G. Holt, "Exploring a vibratory systems analysis of human movement production," *J. Neurophysiol.*, vol. 43, no. 5, pp. 1183–1196, 1980.
- [31] T. Luong, K. Kim, S. Seo, J. H. Park, Y. Kim, S. Y. Yang, K. H. Cho, J. C. Koo, H. R. Choi, and H. Moon, "Impedance control of a high performance twisted-coiled polymer actuator," in *Proc. IEEE/RSJ Int. Conf. Intell. Robots Syst. (IROS)*, Oct. 2018, pp. 8701–8706.
- [32] T. Luong, K. Kim, S. Seo, J. Jeon, J. C. Koo, H. R. Choi, and H. Moon, "Simultaneous position-stiffness control of antagonistically driven twisted-coiled polymer actuators using model predictive control," in *Proc. IEEE/RSJ Int. Conf. Intell. Robots Syst. (IROS)*, Oct. 2020, pp. 8610–8616.
- [33] A. Cherubini, G. Moretti, R. Veretchy, and M. Fontana, "Experimental characterization of thermally-activated artificial muscles based on coiled nylon fishing lines," *AIP Adv.*, vol. 5, no. 6, 2015, Art. no. 067158.
- [34] L. J. Bridgeman, C. Danielson, and S. Di Cairano, "Stability and feasibility of MPC for switched linear systems with dwell-time constraints," in *Proc. Amer. Control Conf. (ACC)*, Jul. 2016, pp. 2681–2686.
- [35] J. Mattingley and S. Boyd, "CVXGEN: A code generator for embedded convex optimization," *Optim. Eng.*, vol. 13, no. 1, pp. 1–27, 2012.
- [36] M. Hanger, T. A. Johansen, G. K. Mykland, and A. Skullestad, "Dynamic model predictive control allocation using CVXGEN," in *Proc. 9th IEEE Int. Conf. Control Autom. (ICCA)*, Dec. 2011, pp. 417–422.
- [37] M. C. Yip and G. Niemeyer, "On the control and properties of supercoiled polymer artificial muscles," *IEEE Trans. Robot.*, vol. 33, no. 3, pp. 689–699, Jun. 2017.
- [38] C. D. Onal and D. Rus, "A modular approach to soft robots," in *Proc. 4th IEEE RAS EMBS Int. Conf. Biomed. Robot. Biomechtron. (BioRob)*, Jun. 2012, pp. 1038–1045.
- [39] H. Logemann, E. P. Ryan, and I. Shvartsman, "A class of differential-delay systems with hysteresis: Asymptotic behaviour of solutions," *Nonlinear Anal., Theory, Methods Appl.*, vol. 69, no. 1, pp. 363–391, 2008.
- [40] W.-C. Su, S. V. Drakunov, and U. Ozguner, "An  $O(T_2)$  boundary layer in sliding mode for sampled-data systems," *IEEE Trans. Autom. Control*, vol. 45, no. 3, pp. 482–485, Mar. 2000.



mobile robot control, as well as machine learning applications.



**SUNGWON SEO** received the B.S. degree in mechanical engineering from Sungkyunkwan University, in 2016, where he is currently pursuing the Ph.D. degree with the Robotics and Intelligent Systems Engineering Laboratory. His current research interests include robot grasping and deep learning for perception.



**KIHYEON KIM** (Student Member, IEEE) received the B.S. degree in mechanical engineering from Sungkyunkwan University, Suwon, South Korea, in 2017, where he is currently pursuing the Ph.D. degree with the School of Mechanical Engineering in the Robotics Innovatory. His research interests include soft robotics and artificial muscles.



**JEONGMIN JEON** received the B.S. degree in mechanical engineering from Sungkyunkwan University, where he is currently pursuing the Ph.D. degree with the Robotics and Intelligent Systems Engineering Laboratory. His current research interests include task and motion planning, machine learning, and mobile manipulation.



**FRANCISCO YUMBRA** received the B.S. degree in electrical engineering specialization in electronics and industrial automation from the Escuela Politecnica del Litoral (ESPOL). He is currently pursuing the Ph.D. degree in mechanical engineering with the Robotics and Intelligent Systems Engineering Laboratory, Sungkyunkwan University (SKKU). His current research interests include combination task and motion planning, and dual-arm manipulation.



**JA CHOON KOO** (Member, IEEE) received the B.S. degree from Hanyang University, Seoul, South Korea, in 1989, and the M.S. and Ph.D. degrees from the University of Texas at Austin, Austin, TX, USA, in 1992 and 1997, respectively, in mechanical engineering, system identification and control, dynamic systems modeling, and simulation. From 1998 to 2001, he was an Advisory Engineer with IBM, San Jose, CA, USA. From 1996 to 1998, he was a Staff Engineer with SISA, San Jose, CA, USA. From 2016 to 2019, he was the Vice President of international affairs, Sungkyunkwan University, Seoul.



**HYOUK RYEOL CHOI** (Fellow, IEEE) received the B.S. degree from Seoul National University, Seoul, South Korea, in 1984, the M.S. degree from the Korea Advanced Institute of Science and Technology (KAIST), Daejeon, South Korea, in 1986, and the Ph.D. degree from the Pohang University of Science and Technology (POSTECH), Pohang, South Korea, in 1994, all in mechanical engineering. From 1986 to 1989, he was an Associate Research Engineer with the IT Research Center, LG electronics. From 1993 to 1995, he was a Postdoctoral Researcher with Kyoto University, Kyoto, Japan. From 1999 to 2000, he was a JSPS Fellow with the National Institute of Advanced Industrial Science and Technology, Japan. From 2008 to 2009, he was a Visiting Professor with the University of Washington, Seattle, WA, USA. Since 1995, he has been a Full Professor with the School.



**HYUNGPIIL MOON** (Member, IEEE) received the B.S. and M.S. degrees in mechanical engineering from the Pohang University of Science and Technology, Pohang, South Korea, in 1996 and 1998, respectively, and the Ph.D. degree in mechanical engineering from the University of Michigan, Ann Arbor, MI, USA, in 2005. From 2006 to 2007, he was a Postdoctoral Researcher with the Robotics Institute, Carnegie Mellon University. In 2008, he joined the Faculty of the School of Mechanical Engineering, Sungkyunkwan University, Suwon, South Korea, where he is currently a Professor. His current research interests include robotic manipulation, SLAM, combined task and motion planning, and polymer-based sensor and actuators. He was a Technical Editor of IEEE/ASME Trans. Mechatronics, and the Editor-in-Chief of *Journal of Korea Robotics Society*. He is also serving as an Editor for ICRA, a Co-Chair for IEEE RAS TC on Robotic Hand, Grasping, and Manipulation, and an Associate Editor for *Intelligent Service Robotics*.

...